NOVEL FREE SURFACE ELECTROSPINNING FOR PREPARING NANOFIBERS AND ITS MECHANISM STUDY

by

Jing YIN and Lan XU *

National Engineering Laboratory for Modern Silk, College of Textile and Clothing Engineering, Soochow University, Suzhou, China

Original scientific paper
https://doi.org/10.2298/TSCI2203527Y

In order to meet the increasing demand for nanofibers and overcome the disadvantages of traditional electrospinning technology, it is necessary to research an electrospinning device that can produce nanofibers efficiently. In this paper, a free surface electrospinning device was improved, and a spherical section free surface electrospinning device was developed to prepare high-quality polyacrylonitrile nanofibers in batches. Meanwhile, MAXWELL 3-D software was used to simulate the electric field distribution of the spherical section free surface electrospinning with solution reservoirs of different spherical radii. The influence of the spherical radius on the spinning effect was analyzed to study the spinning mechanism. The results showed that when the applied voltage was 40 kV, the electric field distribution of the spherical section free surface electrospinning with a larger spherical radius was more uniform, the nanofiber diameter was larger, the nanofiber diameter distribution was more uniform, and the yield of nanofibers was higher. When the spherical radius was 75 mm, the quality of nanofibers was better, and the yield could reach the maximum value of 14.35 g per hour, due to its higher average electric field intensity and uniform electric field distribution.

Key words: *spherical section free surface electrospinning, nanofiber membrane, polyacrylonitrile, electric field distribution*

Introduction

In recent years, nanofibers have been widely used in tissue engineering [1], filter materials [2], sound-absorbing materials [3], wound dressings [4], and food preservation [5] due to their excellent characteristics such as high specific surface area and aspect ratio. At present, the main methods for preparing nanofibers include self-assembly [6], phase separation [7], electrospinning (ES) [1-5], *etc*. The ES is the simplest and lowest cost method that can prepare nanofibers with excellent structure and performance [8]. However, the yield of the traditional single-needle ES (SNE) method was only 0.01-1 g per hour [9], and the needle design is difficult to clean [10].

To overcome the previous shortcomings, some researchers have proposed free surface ES (FSE) technology. The FSE method uses a particular conductive device on the free surface of the liquid to form jets, which is considered that the jets can be formed from any surface [11]. Yarin *et al.* [12] designed an FES device with a two-layer liquid system containing magnetic powders, and its yield of the nanofibers was 12 times higher than that of SNE.

* Corresponding author, e-mail: lanxu@suda.edu.cn

Still, there were magnetic powders in the nanofibers. Forward *et al.* [13] studied a FSE device with a thin wire electrode, and its yield was proved by theoretical values and practical measured data. Tan *et al.* [14] used a FSE device to prepare polyacrylonitrile (PAN)/polyacrylic acid (PAA) nanofibers in batch as the precursor, which were carbonized and used to enhance the sensing performance of carbon nanotubes. Ali *et al.* [15] applied a sawtooth roller device to prepare polyvinyl alcohol (PVA) nanofibers, and combined with electric field analysis, the yield could reach 3.89 g per hour. Keirouz *et al.* [16] presented a high-throughput nozzle FES device to prepare silk fibroin-based fibers, and its yield was 11 times higher than NSE. He [17] developed and designed a bubble electrospinning (BE) using the principle of bubble dynamics, which was simple and available to realize the small-batch preparation of nanofibers. However, the method has some disadvantages such as discontinuous bubble formation, irregular bubble rupture, and uneven of the prepared nanofibers during the spinning process.

In our previous research [18-20], a series of FSE devices for the preparation of nanofibers were developed. A modified BE (MBE) device combining the conical polymer nozzle and copper solution reservoir was presented, and its yield of PVA nanofibers could reach 19.8-72 g per hour [21]. Comparing the preparation mechanism of the MBE, sloping FSE (SFSE), oblique section FSE (OSFSE), and spherical section FSE (SSFSE), the results showed that the uniformity and yield of nanofibers prepared by the SSFSE were the highest [22]. The effects of the solution reservoir radius on the SSFSE processes were investigated, which exhibited the spinning effect was the best when the solution reservoir radius was 25 mm [23].

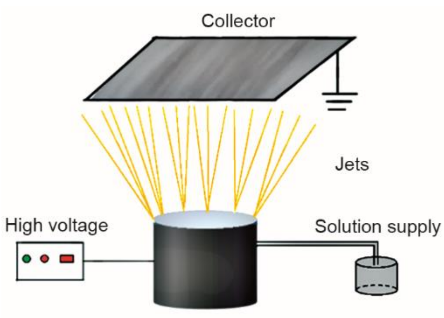

Figure 1. Schematic of the SSFSE device

In this paper, based on the previous works [22, 23], the mechanism of the SSFSE device using a solution reservoir with a radius of 25 mm were further studied. The radius of the sphere truncating the solution reservoir, namely the spherical radius of the solution reservoir, was changed, and the curvature of the spinning working area was changed accordingly. MAXWELL 3-D was used to simulate the electric field distribution of the SSFSE process using solution reservoirs with different spherical radius, and the influence of spherical radius on the quality and yield of polyacrylonitrile nanofibers was studied, which would provide the research foundation for the batch preparation of nanofiber, fig. 1.

Materials and methods

Materials

Polyacrylonitrile (PAN, *Mw* = 15 w) was obtained from Beijing Lark Branch Co., Ltd. (Beijing, China). The N, N-dimethylformamide (DMF) was supplied from Shanghai Chemical Reagent Co., Ltd. (Shanghai, China). 10% PAN were dissolved in DMF under magnetic stirring at 60 °C for four hours to obtain the spinning solution.

Apparatus

Figure 2 illustrates the 3-D schematic diagram and the longitudinal cross-sectional view of the replaceable solution reservoir of the SSFSE device with a height of 40 mm and a diameter of 25 mm, and the curvatures of the working area, K, according to the spherical radii of the solution reservoir, R, are indicated in tab. 1, in which the spherical radius of the solution reservoir is 45 mm, 55 mm, 65 mm, 75 mm, and 85 mm, respectively.

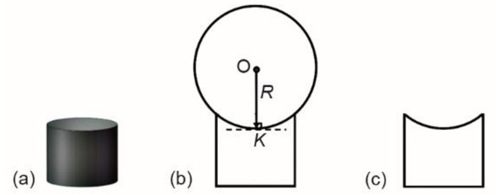

Figure 2. The 3-D schematic diagram (a), the sphere truncating the solution reservoir (b), and the longitudinal cross-sectional view (c) of the replaceable SSFSE solution reservoir

Characterization of nanofibers

Morphology of nanofiber membranes

The SEM (Hitachi S4800, Hitachi, Tokyo, Japan) was used to characterization the morphology of PAN nanofibers. All samples were dried at room temperature and then sputtered with gold through IB-3 (Eiko, Japan) for 90 seconds. And the diameter distribution of nanofibers was carried out using IMAGE J software (National Institute of Mental Health, Bethesda, MD, USA) upon 10 SEM images and measuring 100 nanofibers at random in each SEM image.

Table 1. Parameters of SSFSE device with different spherical radii of the solution reservoirs

R [mm]	45	55	65	75	85
K	0.0222	0.0182	0.0154	0.0133	0.0118

Mechanical properties of PAN nanofiber membranes

The mechanical properties of PAN nanofibers membranes (NFM) were all carried out by a universal electromechanical test machine Instron-3365 (Instron, Norwood, MA, USA). All samples were 40 mm × 10 mm rectangle membranes. The test conditions were a clamping length of 20 mm, a pretension of 0.2 cN and a tensile rate of 100 mm per minute, respectively. Before performing the mechanical tests, these NFM were placed in a constant temperature and pressure chamber and equilibrated for 24 hours to achieve their moisture balance and stabilize the beta-sheet structure of PAN. The measurement was repeated five times.

Yield of nanofiber membranes

The weights of PAN nanofibers produced were measured by a precise electronic balance (XJ120A, Precisa, Shanghai, China) after spinning for 30 minutes and repeated five times to obtain the average value. The calculation method was:

$$W = \frac{W_1 - W_0}{t}$$

where W is the yield of NFM, W_0 and W_1 – the weights of the aluminum foils before and after spinning, respectively, and t – the spinning time.

Simulation of electric field

The electric field distributions from the solution reservoir to the collector were simulated by MAXWELL 3-D. The electric field simulations for these SSFSE processes were using the following experimentally realized experimental parameters: the copper reservoirs as positive pole were all a cylinder with a diameter of 50 mm and a height of 40 mm, which were truncated by spheres with a radius of 45 mm, 55 mm, 65 mm, 75 mm, and 85 mm respectively. The electric conductivity of copper was 5.8×10^{11} μs/cm, the electric conductivity of PAN solution was 918 μs/cm, the applied voltage was 40 kV, and the distance from the surface of the solution to the collector was 180 mm.

To further compare the uniformity of electric field of these five SSFSE processes, a parameter $f = E_{max}/E_{av}$, where E_{max} is the maximum electric field intensity and E_{av} – the average electric field intensity) is introduced [22].

Results and discussion

Morphology of nanofiber membranes

Figure 3 showed the morphology of PAN nanofibers prepared by using SSFSE with different spherical radii of the solution reservoirs, and tab. 2 indicated the corresponding diameter distribution of nanofibers. The results illustrated that all the nanofibers had good morphology, indicating that these self-made SSFSE all had good spinning effects. In addition, as the spherical radius of the solution reservoir increased, the average diameter of the PAN nanofibers increased, and the uniformity of their diameter distribution also increased, due to the weakening of the tip discharge phenomenon and the uniform charge distribution.

Mechanical property

Table 3 shows the mechanical properties of PAN NFM prepared by SSFSE devices with different spherical radii of the solution reservoirs, including the elongation at break and tensile strength. It could be depicted from tab. 3 that with the increase of the spherical radius, the tensile strength of NFM first increased and then decreased, while the elongation at break first decreased and then increased. When the spherical radii of solution reservoir were 75 mm and 85 mm, the tensile strength and the elongation at break of NFM were all relatively larger, due to their large diameter and uniform diameter distribution of nanofibers, as shown in fig. 3 and tab. 2.

Table 2. Diameters of nanofibers with different spherical radii of the solution reservoirs

R [mm]	Average diameter [nm]	Standard deviation [nm]	Confidence internal [nm]
45	228.89	48.35	9.47
55	247.18	43.62	8.55
65	259.62	42.65	8.36
75	262.16	41.43	8.12
85	275.32	41.13	8.05

Table 3. The mechanical property of NFM with different sphere radii

R [mm]	Tensile strength [MPa]	The elongation at break [%]
45	2.564	9.207
55	2.754	5.794
65	4.135	5.209
75	4.499	5.960
85	4.104	7.773

The yield of nanofibers

Figure 4 showed the yield of PAN nanofibers prepared by using SSFSE devices with different spherical radii of the solution reservoirs. The yield of nanofibers first increased and then decreased with the increase of spherical radius. When the spherical radius was 75 mm, the yield of PAN nanofibers reached a maximum of 14.35 g per hour. When the spherical radius was 85 mm, a large number of jets were produced and spread outward due to the highest average electric field intensity. These expanding jets and too high spinning speed made it difficult for nanofibers to be collected on the collector, leading to the decrease of the yield of nanofibers. The results would be explained by simulating the electric field distribution in the SSFSE processes.

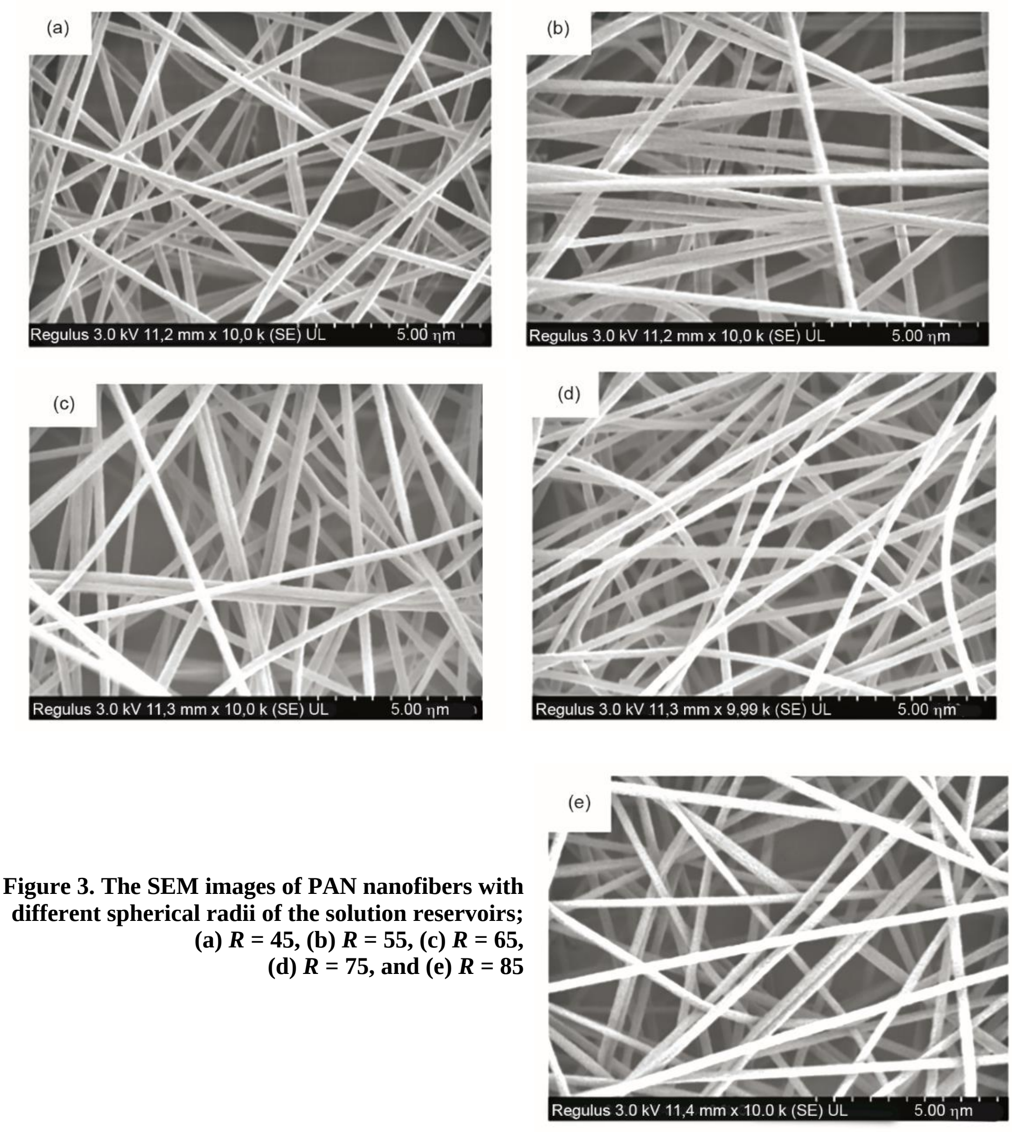

Figure 3. The SEM images of PAN nanofibers with different spherical radii of the solution reservoirs; (a) *R* = 45, (b) *R* = 55, (c) *R* = 65, (d) *R* = 75, and (e) *R* = 85

Simulating electric field

The MAXWELL 3-D was used to simulate the SSFSE processes with different spherical radii. As shown in fig. 5, the vertical view of the electric field intensity of SSFSE devices indicated that the electric field intensity was the largest at the edge of the solution reservoirs. The reason was that the largest curvature of SSFSE device occurred when the spherical radius was 45 mm, which led to more obvious charge accumulation effects on the edge of

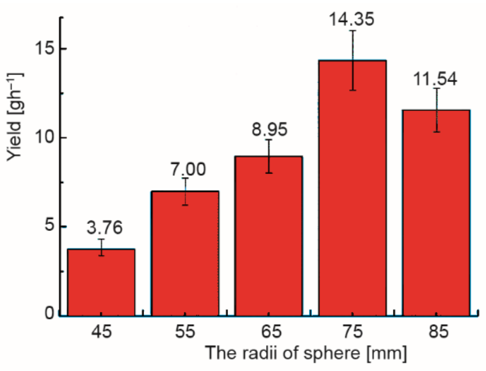

Figure 4. The yields of PAN nanofibers using SSFSE devices with different spherical radii

the solution reservoir. As the distance from the edge of the reservoir increased, the electric field intensity decreased gradually.

Table 4 showed the maximum and average values of the radial electric field intensities in the SSFSE processes with different spherical radii, as well as the corresponding f values. It could be concluded that when the spherical radius was 45 mm the charges are concentrated at the tip, resulting in the largest electric field intensity and the most uneven electric field distribution. The curvature of the spherical section of the solution reservoirs decreased with the increase of spherical radius, and the tip discharge gradually weakened, which made charge diffuses to the center of the solution reservoirs, leading to the improvement of the uniformity of the electric field distribution. The electric field simulation results were consistent with the previous experimental data.

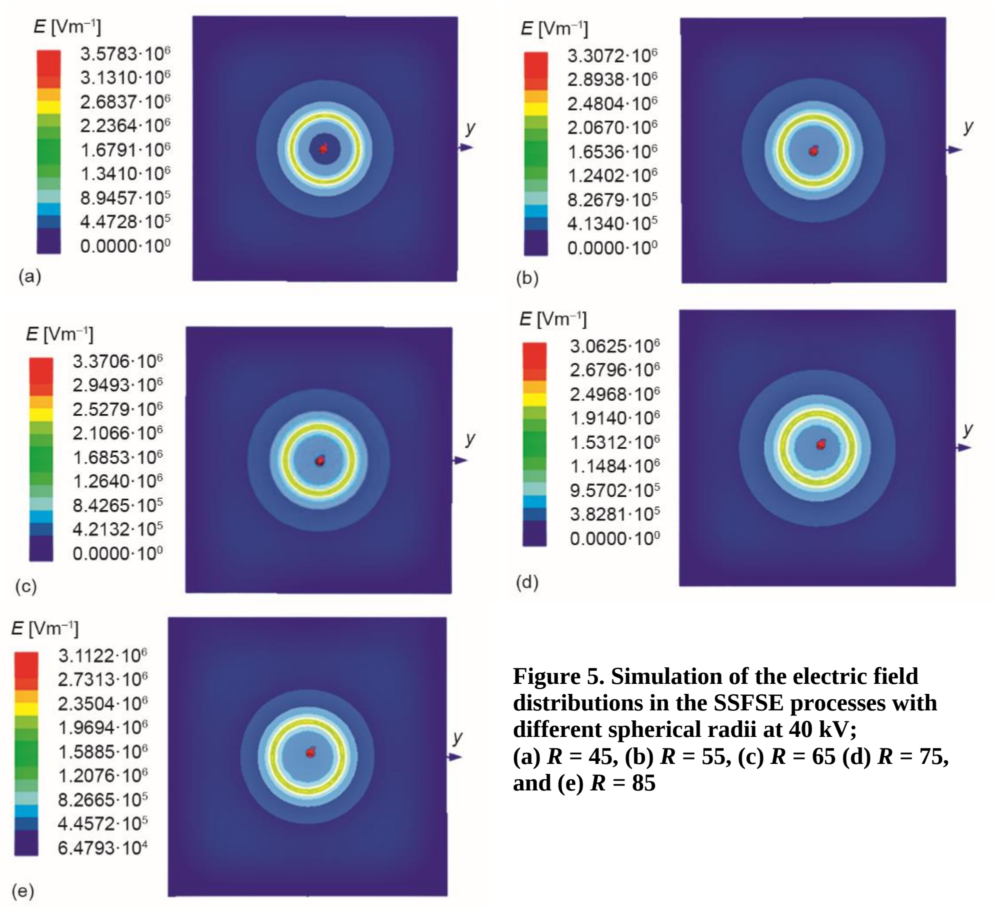

Figure 5. Simulation of the electric field distributions in the SSFSE processes with different spherical radii at 40 kV;
(a) *R* = 45, (b) *R* = 55, (c) *R* = 65 (d) *R* = 75, and (e) *R* = 85

Table 4. Uniformity of electric field intensity at different sphere radii

R	E_{max} [Vm^{-1}]	E_{av} [Vm^{-1}]	f
45	2.34×10^6	5.81×10^5	4.03
55	2.08×10^6	6.0×10^5	3.47
65	2.10×10^6	6.08×10^5	3.45
75	1.93×10^6	6.07×10^5	3.18
85	1.83×10^6	6.09×10^5	3.01

Conclusion

In this paper, the effects of the spherical radius of the SSFSE solution reservoir on the quality and yield of PAN nanofibers were studied. When the spherical radius was 75 mm, the quality of nanofibers was better, and the yield could reach the maximum value of 14.35 g per hour, much higher than those of the traditional electrospinning [24-29]. In addition, numerical simulation and theoretical analysis of the SSFSE devices with different spherical radii were carried out through MAXWELL 3-D software. As the radius of the sphere increased, the uniformity of electric field distribution was improved. And the electric field simulation results were consistent with experimental data, which demonstrated that the SSFSE device with a spherical radius of 75 mm could fabricate PAN NFM with the higher quality and the highest yield at 40 kV due to its higher average electric field intensity and uniform electric field distribution.

Acknowledgment

The work is supported financially by National Natural Science Foundation of China (Grant No. 11672198), Jiangsu Higher Education Institutions of China (Grant No. 20KJA130001), Six Talent Peaks Project of Jiangsu Province (Grant No.GDZB-050), and PAPD (A Project Funded by the Priority Academic Program Development of Jiangsu Higher Education Institutions).

References

[1] Zha, F., *et al.,* Electrospun Natural Polymer and Its Composite Nanofibrous Scaffolds for Nerve Tissue Engineering, *Journal of Biomaterials Science-Polymer Edition, 31* (2019), 4, pp. 519-548
[2] Leung, W. W. F., *et al.,* Electrostatic Charged Nanofiber Filter for Filtering Airborne Novel Coronavirus (COVID-19) and Nano-Aerosols, *Separation and Purification Technology*, *250* (2020), Nov., ID 116886
[3] Huan, L., *et al.*, Structure and Sound Absorption Properties of Spiral Vane Electrospun PVA/PEO Nanofiber Membranes, *Applied Sciences*, *8* (2018), 2, ID 296
[4] Yin, J., *et al.,* Batch Preparation of Electrospun Polycaprolactone/Chitosan/Aloe Vera Blended Nanofiber Membranes for Novel Wound Dressing, *International Journal of Biological Macromolecules*, *160* (2020), Oct., pp. 352-363
[5] Niu, B., *et al.*, Electrospinning of Zein-Ethyl Cellulose Hybrid Nanofibers with Improved Water Resistance for Food Preservation, *International Journal of Biological Macromolecules*, *142* (2020), Jan., pp. 592-599
[6] Zhang, H., *et al.,* A Novel Self-Assembly Approach for Synthesizing Nanofiber Aerogel Supported Platinum Single Atoms, *Journal of Materials Chemistry A*, 8 (2020), 30, pp. 15094-15102
[7] Kang, J., *et al.,* Porous Poly(3-Hydroxybutyrate) Scaffolds Prepared by Non-Solvent-Induced Phase Separation for Tissue Engineering, *Macromolecular Research, 28* (2020), 9, pp. 835-843
[8] Kong, C. S., *et al.,* Nano-Web Formation by the Electrospinning at Various Electric Fields, *Journal of Materials Science*, *42* (2007), 19, pp. 8106-8112

[9] Zhou, Y., *et al.*, Novel Method for Preparation of Continuously Twisted Nanofiber Yarn Based on a Combination of Stepped Airflow Electrospinning and Friction Twisting, *Journal of Materials Science*, *53* (2018), 22, pp. 15735-15745
[10] Liu, Y., *et al.* Homogeneous Field Intensity Control During Multi-Needle Electrospinning *via* Finite Element Analysis and Simulation, *Journal of Nanoscience and Nanotechnology*, *13* (2013), 2, pp. 843-847
[11] Lukas, D., *et al.*, Self-Organization of Jets in Electrospinning for Free Liquid Surface: A Generalized Approach, *Journal of Applied Physics*, *103* (2008), 8, ID 084309
[12] Yarin, A. L., *et al.*, Upward Needleless Electrospinning of Multiple Nanofibers, *Polymer*, *45* (2004), 9, pp. 2977-2980
[13] Forward, K. M., *et al.*, Free Surface Electrospinning from a Wire Electrode, *Chemical Engineering Journal*, *183* (2012), Feb., pp. 492-503
[14] Tan, H. L., *et al.*, High-Throughput Fabrication of Carbonized Electrospun Polyacrylonitrile/Poly (Acrylic Acid) Nanofibers with Additives for Enhanced Electrochemical Sensing, *Journal of Applied Polymer Science*, *137* (2020), 43, ID e49341
[15] Ali, U., *et al.*, Needleless Electrospinning Using Sprocket Wheel Disk Spinneret, *Journal of Materials Science*, *52* (2017), 12, pp. 7567-7577
[16] Keirouz, A., *et al.*, High-Throughput Production of Silk Fibroin-Based Electrospun Fibers as Biomaterial for Skin Tissue Engineering Applications, *Materials science and Engineering C*, *12* (2020), July, ID 110939
[17] He, J. H., Nano Bubble Dynamics in Spider Spinning System, *Journal of Animal and Veterinary Advances*, *7* (2008), 2, pp. 207-209
[18] Shao, Z., *et al.*, Formation Mechanism of Highly Aligned Nanofibers by a Modified Bubble-Electrospinning, *Thermal Science, 22* (2018), 1A, pp. 5-10
[19] Cheng, T., *et al.*, Effect of Surface Active Agent on Bubble-Electrospun Polyacrylonitrile Nanofibers, *Thermal Science*, *23* (2019), 4, pp. 2481-2487
[20] Yin, J., *et al.*, Numerical Approach to High-Throughput of Nanofibers by a Modified Bubble-Electrospinning, *Thermal Science, 24* (2020), 4, pp. 2367-2375
[21] Shao, Z., *et al.*, High-Throughput Fabrication of Quality Nanofibers Using a Modified Free Surface Electrospinning, *Nanoscale Research Letters, 12* (2017), 1, ID 470
[22] Fang, Y., *et al.*, Four Self-Made Free Surface Electrospinning Devices for High-Throughput Preparation of High-Quality Nanofibers, *Beilstein Journal of Nanotechnology*, *10* (2019), 1, pp. 2261-2274
[23] Ahmed, A., *et al.*, High-Throughput Free Surface Electrospinning Using Solution Reservoirs with Different Radii and its Preparation Mechanism Study, *Journal of Materials Research and Technology*, *9* (2020), 4, pp. 9059-9072
[24] Li, X. X., *et al.*, Gecko-Like Adhesion in the Electrospinning Process, *Results in Physics*, *16* (2020), Mar., 102899
[25] Li, X. X., He, J. H., Nanoscale Adhesion and Attachment Oscillation Under the Geometric Potential, Part 1: The Formation Mechanism of Nanofiber Membrane in the Electrospinning, *Results in Physics*, *12* (2019), Mar., pp.1405-1410
[26] Peng, N. B., He, J. H., Insight into the Wetting Property of a Nanofiber Membrane by the Geometrical Potential, *Recent Patents on Nanotechnology*, *14* (2020), 1, pp. 64-70
[27] Tian, D., *et al.*, Macromolecule Orientation in Nanofibers, *Nanomaterials, 8* (2018), 11, 918
[28] Tian, D, He, J. H., Control of Macromolecule Chains Structure in a Nanofiber, *Polymers*, *12* (2020), 10, 2305
[29] Tian, D., *et al.*, Electrospun Mussel-derived Silk Fibers, *Recent Patents on Nanotechnology, 14* (2020), 1, pp. 14-20

Paper submitted: August 18, 2020
Paper revised: March 18, 2021
Paper accepted: March 18, 2021